Available online at www.sciencedirect.com
SCIENCE DIRECT®
International Journal of Heat and Mass Transfer 48 (2005) 3982–3994
International Journal of HEAT and MASS TRANSFER
www.elsevier.com/locate/ijhmt

Effects of rotation on natural convection cooling from three rows of heat sources in a rectangular cavity

L.F. Jin [a], K.W. Tou [a], C.P. Tso [b,*]

[a] School of Mechanical and Production Engineering, Nanyang Technological University, 50 Nanyang Avenue, Singapore 639798, Singapore
[b] Faculty of Engineering and Technology, Multimedia University, Jalan Ayer Keroh Lama, 75450 Melaka, Malaysia

Received 24 August 2004; received in revised form 15 April 2005

Abstract

Two-dimensional unsteady numerical studies are made on an air-filled enclosure rotated about its horizontal axis with an array of three rows of heat sources on one of the walls, revealing three physically realizable phenomena, namely, uni-periodic oscillation, multi-periodic oscillation and chaotic oscillation. The evolutionary process of flow field and natural convection characteristics from stationary to rotating situation is studied. Rotation results in an imbalance between clockwise and counter-clockwise circulations, increases heat transfer in the worst scenario, reduces the oscillation of Nusselt number, and improves or reduces mean performance in each cycle. The optimal distribution of heaters in rotating fluid is close to the results in the stationary situation if they have same dominated circulation direction.

Keywords: Rotating cavity; Discrete heat sources; Natural convection; Electronics cooling

1. Introduction

Electronics cooling under natural convection has been studied by many [1–6], the common model being the discrete heat sources in a rectangular enclosure. With advanced technology, thermal management in the unsteady or rotating condition may be encountered in such situations as rotary machines, guided missiles and space-based manufacturing processes. Bobco [7] introduced the application of natural convection in the design of a vented Gallileo mission descent module parachuting into the Jupiter atmosphere. It was reported [8] that the failure caused by temperature and vibration amounts to 75% of all failures. There had been many studies on flow in rotating ducts, for instance in relation to cooling of turbine blades [9]. However, there are limited studies in unsteady natural convection cooling from discrete heat sources in rotation. The situation with natural convection is very different from forced convection because the latter is pressure-driven flow where the centrifugal force plays an important role and the thermal buoyancy effect is neglected. In a sense, there is no absolute stationary state on earth, since Taylor number, normally used to reflect the effect of Coriolis force in the rotating fluid, is about unity at the equatorial sea level [10]. This is the motivation of the present investigation on the effects of rotation on the periodical behavior of natural convection cooling from three rows of heat

* Corresponding author. Tel.: +606 252 3075; fax: +606 231 6552.
E-mail address: cptso@mmu.edu.my (C.P. Tso).

0017-9310/$ - see front matter © 2005 Elsevier Ltd. All rights reserved.
doi:10.1016/j.ijheatmasstransfer.2005.04.013

Nomenclature

A_H, A_W	aspect ratio along x- and y-direction
d, d'	distance between side heater and center heater, m
$\vec{g}$	gravitational acceleration vector, m^2/s
g	magnitude of gravitational acceleration, m^2/s
H	the side of the enclosure, m
k	thermal conductivity, W/m K
L	heater length, m
L_1, L_2	enclosure heater location, m
n	rotation number for one periodic cycle
Nu, $\overline{\overline{Nu}}$	Local Nusselt number
$\overline{Nu}$, $\overline{\overline{Nu}}$	space averaged and time and space averaged Nusselt number
Nu_i	Nusselt number for heater of i row
Nu_{max}, Nu_{min}	maximum and minimum Nusselt number
p, p_m	pressure and motion pressure, Pa
P	dimensionless motion pressure
Pr	Prandtl number
q''	heat flux, W/m^2
Ra	Rayleigh number
Ra^*	modified Rayleigh number
Ra_w	rotation Rayleigh number
t	time, s
T	temperature, K
Ta	Taylor number
T_c	temperature of the cold wall, K
u, v	dimensional velocity components, m/s
U, V	dimensionless velocity components
$\vec{V}$	velocity vector, m/s
W	enclosure width, m
x, y	dimensional Cartesian coordinate system, m
X, Y	dimensionless Cartesian coordinate system

Greek symbols

α	thermal diffusivity, m^2/s
β	thermal expansion coefficient, 1/K
θ	dimensionless temperature
ν	kinematic viscosity, m^2/s
ρ_0	density at the mean temperature, kg/m^3
ϕ	angular position of cavity, °
ϕ_1, ϕ_2, ϕ_3	angular position of the first, second, and third inflexion, °
τ	dimensionless time
τ_0	dimensionless time for one rotation
$\Delta\tau$	dimensionless time step (variable)
Ω	angular rotation rate vector, rad/s
Ω	magnitude of angular rotation rate, rad/s

sources in a rectangular cavity, extending our earlier work on the stationary cavity [6,11,12].

Although a detailed 3-D numerical computation for this discrete heat sources condition is formidable, especially with the influence of the buoyancy force, Coriolis force and centrifugal force all within the same frame when the cavity is rotated, it is still challenging and useful to study a 2-D model. For the present geometry it will be shown that the results are close to 3-D results. Comparison will be made with reported work on uniform wall temperature condition [13] and physical explanations of results given wherever possible. An attempt will also be made to obtain an optimal heater spacing design criterion.

2. Numerical methodology and validation

2.1. Governing equations and boundary conditions

The geometry and boundary conditions are shown in Fig. 1. The enclosure, filled with air, executes a steady uniform counterclockwise angular velocity about a horizontal axis. (The rotation axis is vertical to the XOY plane.) Three discrete rows of heat source are flushed-mounted onto one of the side walls, while the opposite wall acts as a uniform temperature cold surface. The remaining walls are insulated from the surroundings. This model can be tracked to studies in stationary cases [2–6,11,12,14].

The non-inertial reference frame XOY is shown in Fig. 1. Boussinesq approximation is widely used in natural convection [3–6,9–13,15–18] and the justification for rotating fluids can be found in [15,16]. Then the terms representing the thermal and rotational buoyancies and Coriolis force are, respectively, equal to $\rho_0 \vec{g}\,\beta(T-T_c)$, $-\rho_0\beta(T-T_c)\,\Omega\times(\Omega\times\vec{r})$ and $-2\rho_0[1-\beta(T-T_c)]\,\Omega\times V$. Using L, α/L, L^2/α, $\alpha^2\rho_0/L^2$ and $q''L/k$ as scales for length, velocity, time, pressure and temperature, respectively, the dimensionless variables are defined as

$$\left.\begin{aligned} &X=\frac{x}{L},\quad Y=\frac{y}{L},\quad U=\frac{uL}{\alpha},\quad V=\frac{vL}{\alpha},\\ &\tau=\frac{t\alpha}{L^2},\quad P=\frac{p_mL^2}{\alpha^2\rho_0},\quad \theta=\frac{T-T_c}{q''L/k},\\ &Ra_\omega=\frac{\beta\Omega^2L^5q''}{k\alpha\nu},\quad Ra^*=\frac{g\beta L^4q''}{k\alpha\nu},\\ &Ta=\frac{4\Omega^2L^4}{\nu^2},\quad Pr=\frac{\nu}{\alpha},\\ &A_W=\frac{W}{L},\quad A_H=\frac{H}{L}, \end{aligned}\right\} \tag{1}$$

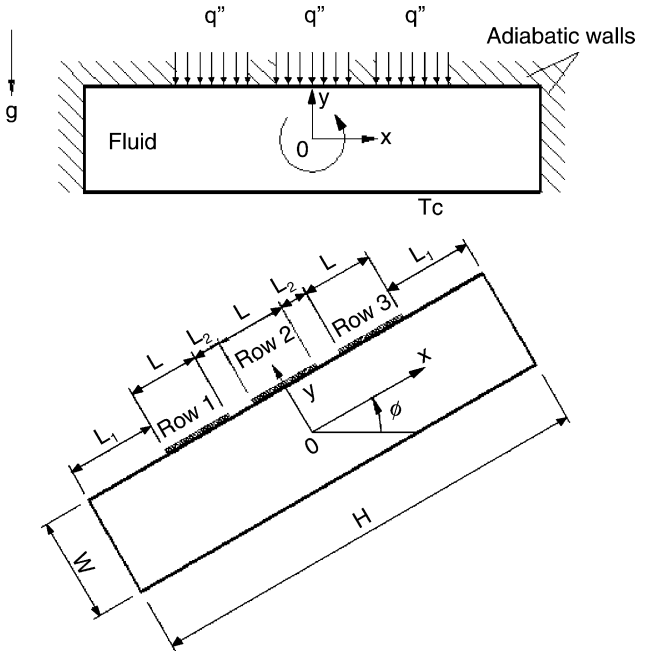

Fig. 1. Physical and geometrical arrangement.

where the motion pressure is defined as

$$P_m = p - \frac{1}{2}\rho_0\Omega^2x^2 - \frac{1}{2}\rho_0\Omega^2y^2 + \rho_0 gx\sin(\Omega t) + \rho_0 gy\cos(\Omega t). \quad (2)$$

As mentioned by Vanyo [17], in a rotating Eulerian coordinate system, the centripetal term can be included in the pressure term and disappears from the typical rotating fluid computation. With Boussinesq approximation, the main part of the centrifugal force term is combined with the pressure term and others are caused by density change and centrifugal buoyancy. In most cases, if the change of density is small and the rotation speed is low ($\omega^2 r/g) \ll 1$, the effect of this term can be neglected completely [13], and this is verified in the present studies.

With a selected coolant, Prandtl number (Pr) is assumed fixed and there are two physical variables, heat flux and rotation speed, which are reflected by the modified Rayleigh number (Ra^*) and Taylor number (Ta), respectively. Due to the rotation Rayleigh number (Ra_w) not being an independent parameter but dependent on Ra, Pr, and Ta, we will not discuss Ra_w except in specifying it explicitly. The Coriolis buoyancy force is neglected, due to $|\beta(T - T_c)| \ll 1$ in present studies. Then the dimensionless governing equations and boundary conditions are as the following:

Continuity equation:

$$\frac{\partial U}{\partial X} + \frac{\partial V}{\partial Y} = 0. \quad (3)$$

Momentum equations:

$$\frac{\partial U}{\partial \tau} + U\frac{\partial U}{\partial X} + V\frac{\partial U}{\partial Y} = -\frac{\partial P}{\partial X} + Pr\left[\frac{\partial^2 U}{\partial X^2} + \frac{\partial^2 U}{\partial Y^2}\right] + \underbrace{Ta^{0.5}PrV}_{\text{Coriolis force term}} - \underbrace{Ra_\omega PrX\theta}_{\text{Centrifugal force term}} + \underbrace{Ra^*Pr\theta\sin(0.5Ta^{0.5}Pr\tau)}_{\text{Buoyancy force term}}, \quad (4)$$

$$\frac{\partial V}{\partial \tau} + U\frac{\partial V}{\partial X} + V\frac{\partial V}{\partial Y} = -\frac{\partial P}{\partial Y} + Pr\left[\frac{\partial^2 V}{\partial X^2} + \frac{\partial^2 V}{\partial Y^2}\right] - \underbrace{Ta^{0.5}PrU}_{\text{Coriolis force term}} - \underbrace{Ra_\omega PrY\theta}_{\text{Centrifugal force term}} + \underbrace{Ra^*Pr\theta\cos(0.5Ta^{0.5}Pr\tau)}_{\text{Buoyancy force term}}. \quad (5)$$

Energy equation:

$$\frac{\partial \theta}{\partial \tau} + U\frac{\partial \theta}{\partial X} + V\frac{\partial \theta}{\partial Y} = \frac{\partial^2 \theta}{\partial X^2} + \frac{\partial^2 \theta}{\partial Y^2}. \quad (6)$$

Boundary conditions:

$$\left.\begin{array}{l} \text{At } X = -A_H/2 : U = V = 0,\ \dfrac{\partial \theta}{\partial X} = 0, \\ \text{At } X = A_H/2 : U = V = 0,\ \dfrac{\partial \theta}{\partial X} = 0, \\ \text{At } Y = A_W/2 : U = V = 0, \\ \quad \dfrac{\partial \theta}{\partial Y} = -1 \quad \text{for the iso-flux regions (heaters)}, \\ \quad \dfrac{\partial \theta}{\partial Y} = 0 \quad \text{for the insulated regions}, \\ \text{At } Y = -A_W/2,\ U = V = 0,\ \theta = 0. \end{array}\right\} \quad (7)$$

To examine the time evolution of the velocity and temperature fields, results for local, space-averaged and time-space-averaged Nusselt number ($Nu, \overline{Nu}, \overline{\overline{Nu}}$) can be evaluated from

$$\left.\begin{aligned} Nu(Y)|_{\phi=\varphi} &= \frac{1}{\theta(Y)}\bigg|_{\phi=\varphi} = \frac{q''L}{K\cdot[T(Y)-T_c]}\bigg|_{\phi=\varphi}, \\ \overline{Nu_i}\big|_{\phi=\varphi} &= \frac{q''L}{\int_L K\cdot[T(Y)-T_c]\,dX}\bigg|_{\phi=\varphi}, \quad i=1,2,3, \\ \overline{Nu}\big|_{\phi=\varphi} &= \left[\sum_{i=1}^{3}\frac{q''L}{\int_L K\cdot[T(Y)-T_c]\,dX}\bigg|_{\phi=\varphi}\right]\Big/3, \\ \overline{\overline{Nu_i}} &= \frac{\int_0^{2n\pi} Nu_i\,d\phi}{2n\pi} \quad \text{(averaged over one cycle)}, \\ \overline{\overline{Nu}} &= \left(\sum_{i=1}^{3}\overline{\overline{Nu_i}}\right)/3. \end{aligned}\right\} \tag{8}$$

2.2. Solution method

For this unsteady problem, first-order implicit scheme is used for the unsteady term and the other numerical procedures of finite volume method are the same as reported previously [6,12]. The steady-state result for each step is obtained by two convergence criteria: (1) $\mathrm{SMAX} \leqslant 1\times10^{-10}$, and (2) $\mathrm{MAX}(\theta_{i,j}^{n+1}-\theta_{i,j}^{n}) \leqslant 1\times10^{-5}$. SIMPLE arithmetic is adopted to solve the coupled velocity and pressure. In the iteration procedure, the motion pressure correction equations are used to derive the new velocity from the previous calculated velocity. SMAX is the largest absolute value of the "mass source" used in the motion pressure correction equations and $\mathrm{SMAX} \leqslant 10^{-10}$ is used as the velocity convergence criterion. The numerical oscillations required to reach the final state varies from 10 to 200 rotations. The $\Delta\tau$, τ_0 are the dimensionless time step in numerical simulations and dimensionless time required for one rotation circulation, respectively. In present studies, $\Delta\tau$ equals $1/72\tau_0$.

Some simulations may require up to one week of computational time with a Pentium IV PC. For example, if we use 20×90 mesh grids, it may take only one minute to get one convergence result for the steady problem. Uniform grid is used in the x-direction, while a non-uniform grid distribution with the characteristic of fine mesh at the two sides and coarse mesh in the middle zone is used in the y-direction of the computation domain, in order to capture the surface heat transfer without bringing about too many grid points. The mesh lengths are increased gradually from the finer mesh, in the ratio 1:1.1, to match smoothly with the coarse mesh. However, for the present unsteady problem, 72 time steps are used in each rotation circulation and 175 circulations are necessary to ensure that the final periodic condition has been reached, as shown in Fig. 4(c). Then the total computation time is estimated to be $1\times72\times175=12\,600$ min $=8.75$ days. If 360 time steps are used in each rotation circulation that is necessary in high Taylor number, it will take more than one month of computation time. Therefore, only 2-D numerical simulations are adopted and the work is confined to studying the periodic field in natural convection.

2.3. Numerical validations

In view of the complex flow to be simulated, stringent tests are conducted. First, computations are carried out for cases at various stationary ($\Omega=0$) orientations shown in Fig. 11 in [12]. Without edge effects, the results of 2-D model are close to those of 3-D model. Therefore, 2-D model can be used without losing generality in the stationary case. Next, tests are performed for a rotating cavity of square cross-section with constant temperature at the hot wall and cold wall. Compared with forced convection, velocity gradient of natural convection is low since normally the maximum velocity magnitude is about 10^{-2}–10^{-1} m/s and the flow not of the boundary layer type. However, the temperature gradient is relative high and the periodic temperature fields are easier to be measured successfully than flow fields. Therefore, validation of the program and most discussion are based on temperature results. As shown in Fig. 2, at different orientations and rotation speeds, close agreement is obtained when compared with results of Hamady et al. [13] who used the same governing equation, and this gives confidence to our simulation results.

We have also carried out experimental studies using the setup in [12] and changed the program code to consider those experimental conditions, and they will be reported separately. Here, a brief comparison with the experimental results is presented in Fig. 3, where the heater aspect ratio equals 6. The comparison shows similar trends and the maximum deviation between them is less than 15%. These show that 2-D model can be valid in applications when the heater aspect ratio is high and the effect of rotation is relatively low. Finally, some grid-independence tests are conducted. The differences in $\overline{Nu_i}$, $\overline{Nu}$ predicted from the original grid (20×90) and finer grid (40×120) are within 1% during the entire periodic oscillation, with differences in the last temperature field kept within 2%. Different time steps $\Delta\tau$ up to $(1/360)\tau_0$ are used to ensure convergence when Ta is higher than 10^3. Through these tests, the present numerical method is considered suitable for the present problem.

3. Results and discussion

The study fields are shown in Table 1.

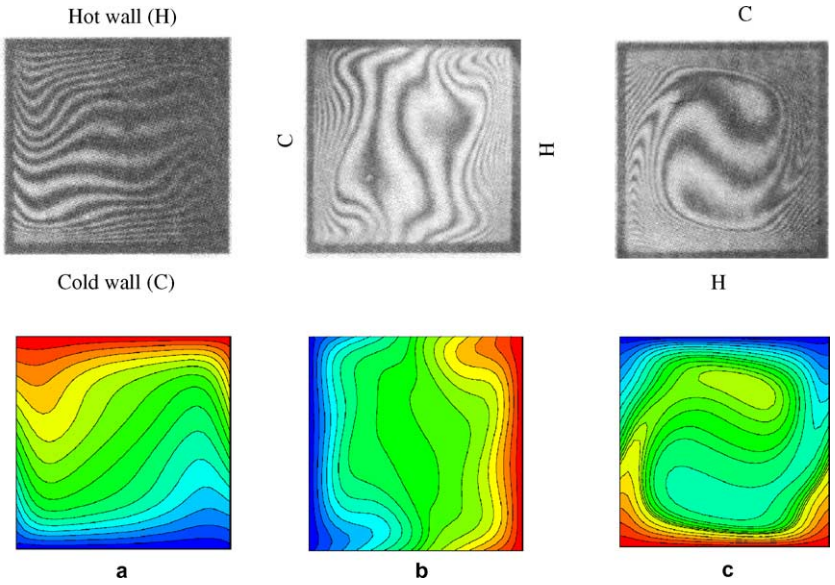

Fig. 2. Comparison of computed isotherms with experiment results of [13] shown in the upper figures ($Ra = 3 \times 10^5$, $Pr = 0.7$): (a) $\phi = 0°$, $\Omega = 17.5$ rpm; (b) $\phi = 270°$, $\Omega = 15.5$ rpm; (c) $\phi = 180°$, $\Omega = 17.5$ rpm.

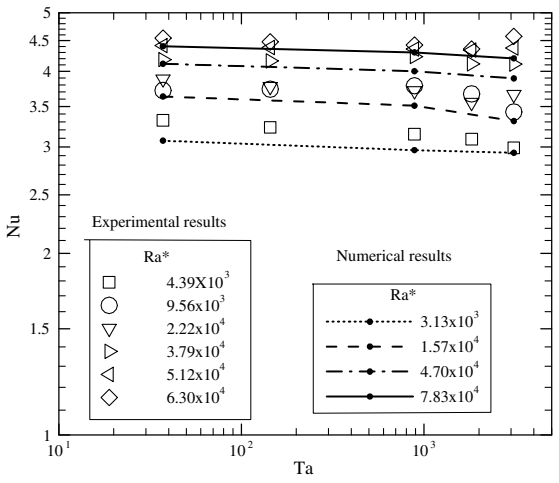

Fig. 3. Brief comparison between numerical and experimental results.

Table 1
Summary of model parameters

Ra^*	Ta	Pr	A_W	A_H
10^3–10^7	0–10^4	0.7	1, 2	7.5

Note: Heater length, $L = 12.7$ mm.

3.1. Oscillation phenomena

Under a non-inertial frame, the driving buoyancy force rotates in the enclosure and results in an oscillation phenomenon. When the time for one cycle equals the time for finishing one rotation, it is uni-rotation periodic oscillation ($n = 1$), otherwise it is multi-rotation oscillation ($1 < n < \infty$).

Typical result for uni-rotation periodic oscillation problem is shown in Fig. 4(a), where after about five rotations ($\tau = 5\tau_0$), the final periodic oscillation pattern is obtained. To ensure correct results, additional computation was carried out beyond five rotations. Fig. 4(b) shows the Nu evolution for multi-rotating periodic oscillation. With the same Ra^* and increased Ta, chaotic oscillation occurs as shown in Fig. 4(c) where even after 175 rotations, there is still no sign of periodic oscillation. At the special values of flow parameters, the flow may have different features, i.e., periodic oscillating or chaotic oscillating flows, similar to observations reported in a numerical study of combined free and forced convection in a rotating curved duct [18].

3.2. Flow and temperature fields with rotation

Due to the close relationship between stationary and low rotation case, the discussion will begin with the stationary case first. In the vertical orientation, $\phi = 90°$ (270°), the enclosure is filled with strong uni-cellular clockwise-circulation (counter-clockwise-circulation). In the orientations that ϕ is close to 0° or 180°, there are different multi-cellular flow patterns shown in Table 2 of [12], with both clockwise and counter-clockwise vortices present, and this can be treated as the transition stage between clockwise-circulation and counter-clockwise-circulations. In particular, in the orientation that

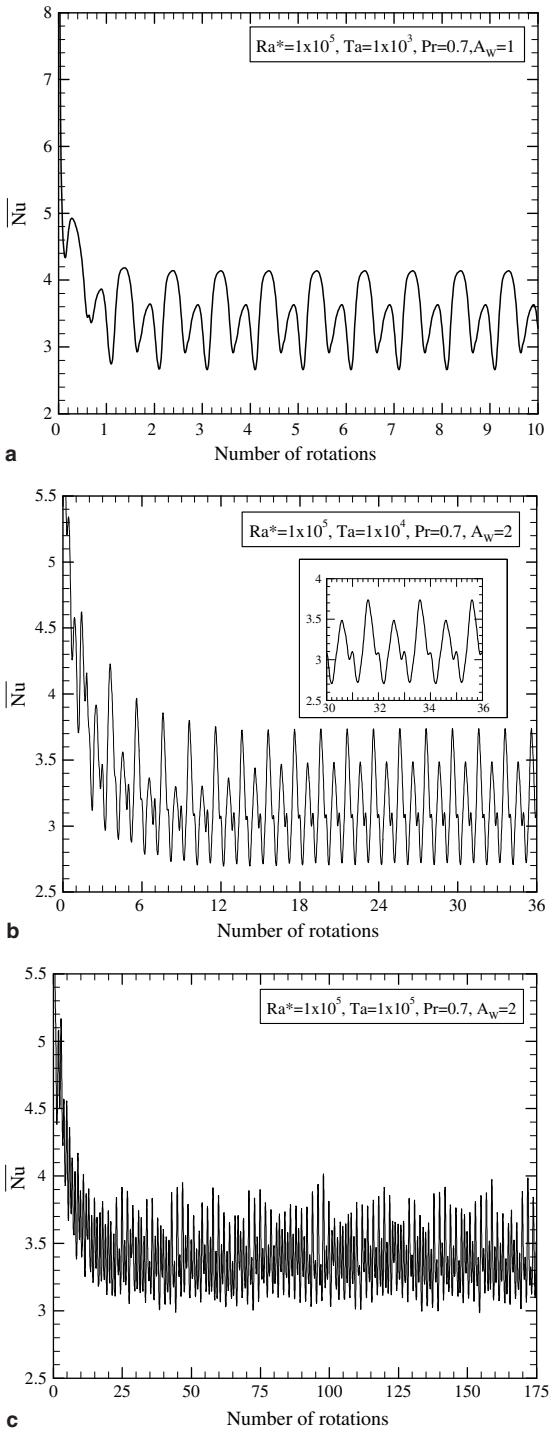

Fig. 4. Three physically realizable oscillations: (a) uni-rotation periodic oscillation; (b) multi-rotation periodic oscillation; (c) chaotic oscillation.

ϕ equals 0° or 180°, the strengths of the two circulations equal each other and the flow and temperature fields are symmetric. In the whole cycle ($\phi = 0$–360°), the flow and temperature fields are in reversed symmetry with respect to 180°. From scale analysis [12], the clockwise or counter-clockwise circulation is dominated by buoyancy force and friction force.

Flow and temperature fields at the onset of rotation are shown in Figs. 5 and 6. There are two uneven vortices in Fig. 5(a) as a result of transition from counter-clockwise to clockwise circulation, with clockwise motion appearing stronger. And in the temperature field, the convective heat transfer resulted from clockwise motion can be seen clearly. Therefore, a higher *Nu* is expected compared to the stationary case where thermal conduction dominates. In Fig. 5(b) ($\phi = 45°$), even though the clockwise motion dominates the flow, the temperature field shows hierarchical structure and results in an expected local minimum *Nu*, shown in Fig. 7 for the circle line of $Ta = 10^3$. However, it is different from conduction domination where *Nu* is close to unity. From Fig. 5(c) to Fig. 6(a), clock-wise motion dominates the flow, but in Fig. 6(b) ($\phi = 225°$), the flow enters the transition stage again. In the core region, counter-clockwise circulation appears and becomes increasingly stronger. The clockwise circulation falls back to the corner regions and becomes weakened until obliterated finally. In this orientation or near it, hierarchical structure re-appears and brings about the second local minimum Nusselt number. In the transition stage, there are more vortices in the cavity that cause difficulties in numerical simulations. After the transition stage, the counter-clockwise motion dominates the flow as shown in Fig. 6(d), but it is not as strong as the earlier dominant clockwise motion. The flow and temperature field for the phase angle of 360° is the same as that for 0°, thus completing a periodic process. The rotation-induced symmetry-breaking phenomenon is mainly caused by the inertial force. With the increase in rotation and hence inertial force, the counter-clockwise circulation will disappear at last, as discussed in the next section.

3.3. Effects of rotation to heat transfer

For the stationary case, as shown by the mean Nusselt number results with zero *Ta* in Figs. 7 and 8(a), three phenomena can be seen: (1) There are three local peaks in one period. The two side-peak values are responding to the strongest points of clockwise and counter-clockwise motions while the middle value is the result of Rayleigh–Benard convection. (2) Corresponding to the three local peaks, there are three inflexion points and the angles at the inflexion points are shown in Table 2 as ϕ_1, ϕ_2, ϕ_3. (3) The minimum *Nu* of 1.76 is closer to unity due to conduction heat transfer. The effects due to rotation are summarized in Table 2.

For the stationary and low rotation cases, thermal buoyancy force causes two or more local peaks in *Nu*,

Table 2
Effects of rotation ($Ra^* = 1 \times 10^5$, $Pr = 0.7$)

Ta	No. of peak Nu	Nu_{max}	Nu_{min}	ΔNu ($Nu_{max}-Nu_{min}$)	ϕ_1	ϕ_2	ϕ_3
0	3	4.520	1.760	2.76	~0°	~160°	~200°
10^3	2	4.139	2.660	1.479	~30°	~225°	
10^4	2	3.586	2.549	1.037	~85°	~305°	
10^5	1	3.577	3.065	0.512	~135°		

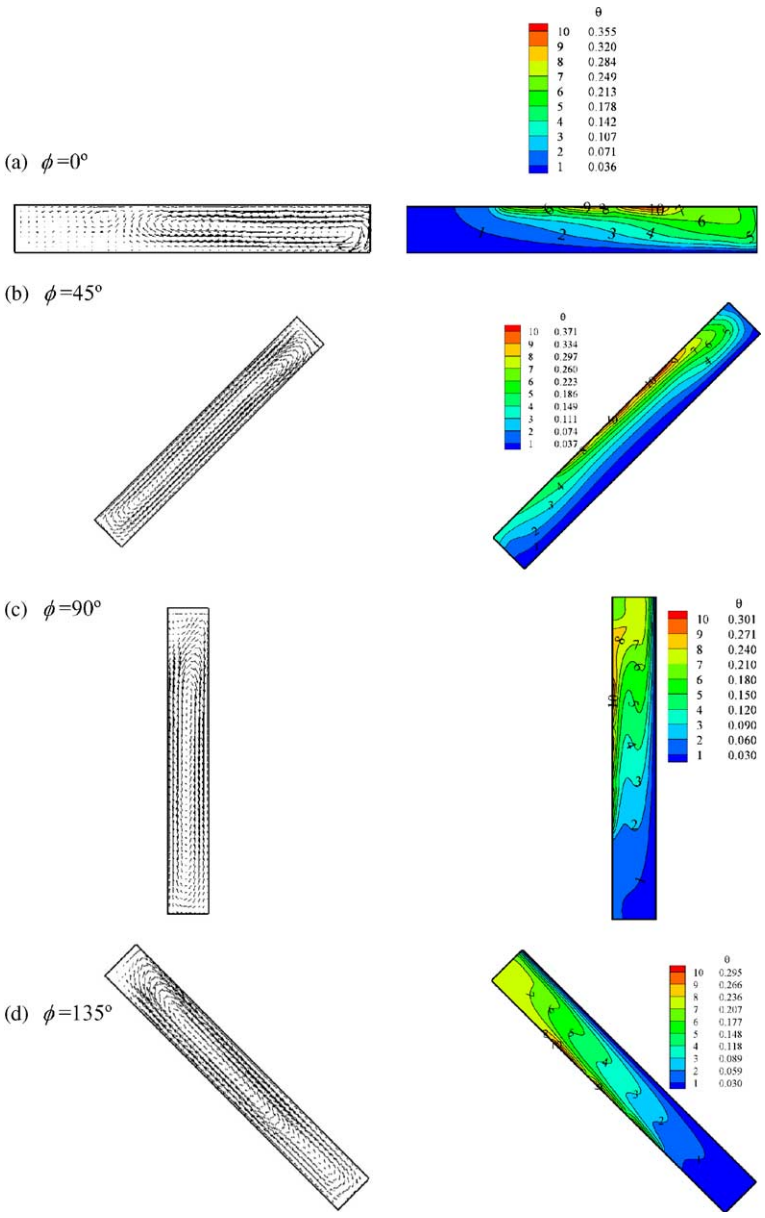

Fig. 5. First part of flow and temperature fields with rotation ($Ra^* = 1 \times 10^5$, $Ta = 1 \times 10^3$, $Pr = 0.7$, $A_W = 1$).

and the flow consists of clockwise circulation, counter-clockwise circulation and two transition stages between them. With the increase in rotation speed, the clock-wise circulation is enlarged and tends to cover the other

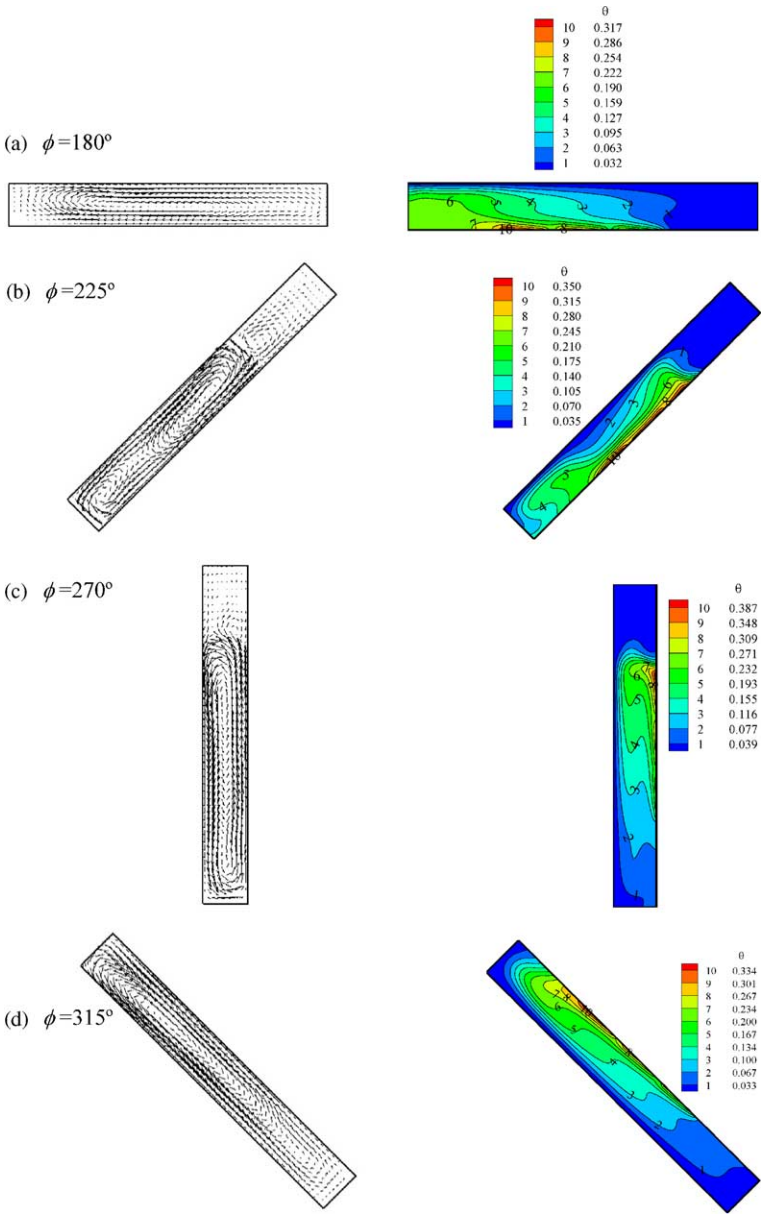

Fig. 6. Second part of flow and temperature fields with rotation ($Ra^* = 1 \times 10^5$, $Ta = 1 \times 10^3$, $Pr = 0.7$, $A_W = 1$).

circulations. As a result, except for the first local peak *Nu*, the others become weakened and disappeared when the rotation speed is high enough. In Fig. 7, it can be seen that with increasing rotation and *Ta*, the swing of *Nu* is reduced and the minimum *Nu* is improved (increased) gradually. The continuous line ($Ta = 10^5$) in Fig. 7 shows that the flow is dominated by clockwise circulation. Correspondingly, there is only one peak and valley for *Nu*. This shows that the inertial force plays an important role in rotating fluids, similar to earlier observations in [13].

The Fig. 8 shows that the heat transfer behavior of row 1 and row 3 are not in reversed symmetry and they become asymmetrical gradually with the increase of rotation speed and Taylor number, resulting from the evolutionary process in the flow and temperature fields.

In Fig. 9, the multi-rotation periodic oscillation is shown. It should be pointed out this has the same Ra^* and *Ta* as the indented line in Fig. 7, and the only difference is the value of the aspect ratio, A_W. With increasing rotation speed, chaotic oscillation, as shown in Fig. 4(c) will take place.

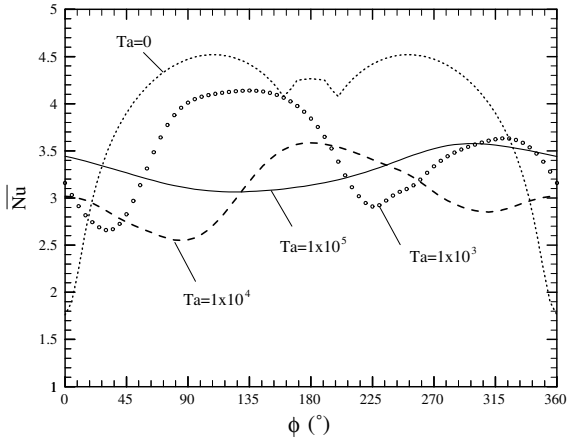

Fig. 7. Effects of Taylor number ($Ra^* = 1 \times 10^5$, $Pr = 0.7$, $A_W = 1$).

3.4. Effects of heat flux to heat transfer

The effects of heat flux to heat transfer can be obtained with a fixed Ta and different Ra^*, as shown in Figs. 10 and 11. When Ra^* is as low as 10^3, conduction heat transfer with characteristics of low and flat Nu is seen. When Ra^* is increased to 10^4, the fluctuation of Nu indicates the onset of convection and there is only one peak Nu. Further increase in Ra^* shows more oscillations in Nu and two or three local peaks Nu appear in Fig. 10. These evolution phenomena seem like a reverse process as discussed earlier on Fig. 7 and Table 3, showing that the process is affected by the combined effect of rotation and heat flux.

3.5. Effects of rotation to time-and-space averaged heat transfer

Fig. 12 shows that rotation delays the onset of convection, agreeing with the findings of Fernando and Smith [19]. This is especially clear when Ta is as high as 10^4. As a result of continuity, rotation reduces heat transfer performance in the low rotation speed range and increases it in the relatively high speed ranges. The summary of correlations of $\overline{\overline{Nu}}$ as a function of Ra^*, at different Ta, is shown in Table 3.

3.6. Optimal distribution of discrete heat sources

A design process requires the evaluation of a number of available options to determine the most appropriate case that meets the primary design requirement, e.g., maximum mean heat transfer, or minimum peak temperature in the system. For natural convection, constrains come not only from computational challenges, but also design and manufacture requirements. An attempt is now given to determine the optimal distribution of the discrete heat sources using the present model.

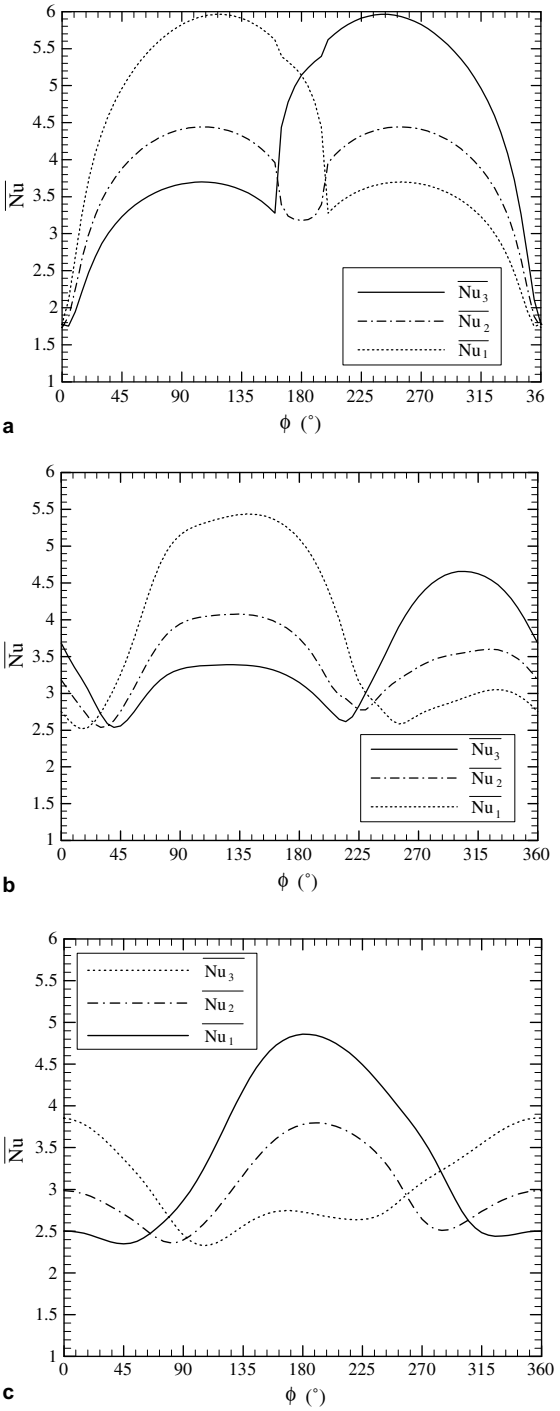

Fig. 8. Mean Nusselt number for each row of heater at different Taylor number ($Ra^* = 1 \times 10^5$, $Pr = 0.7$, $A_W = 1$): (a) $Ta = 0$, (b) $Ta = 1 \times 10^3$, (c) $Ta = 1 \times 10^4$.

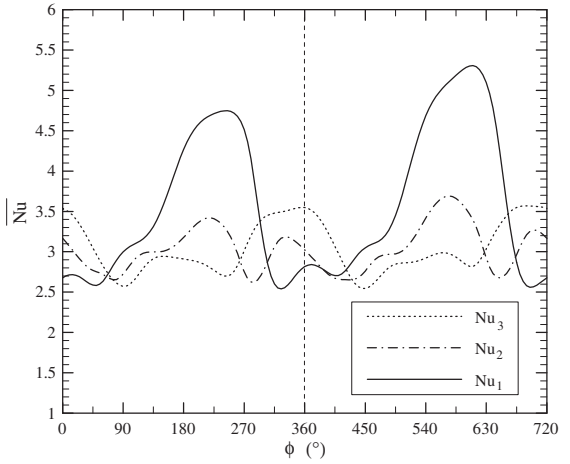

Fig. 9. Mean Nusselt number for each row of heater for multi-rotation oscillation ($Ra^* = 1 \times 10^5$, $Ta = 1 \times 10^4$, $Pr = 0.7$, $A_W = 2$).

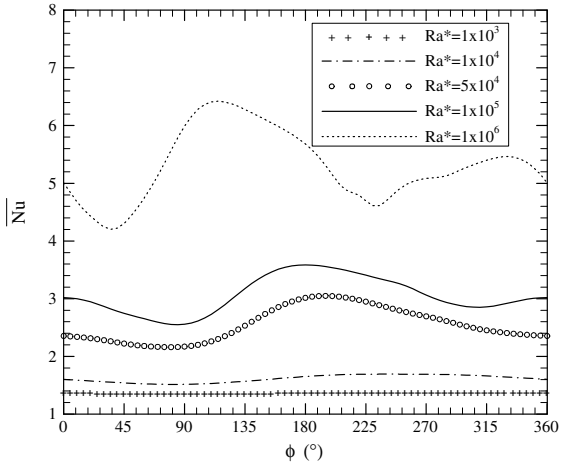

Fig. 10. Effects of modified Rayleigh number ($Ta = 1 \times 10^4$, $Pr = 0.7$, $A_W = 1$).

For the facility of discussion, two new dimension variables, d and d', related to geometrical configuration are shown respectively in Figs. 13 and 15. Firstly, calculations are carried out when the middle heater is fixed at the center line of the wall and the locations of the two side heaters are changed symmetrically. From Fig. 13, even though minimization is the developmental trend of electronics packaging, greater distance between the side heater and middle heater will result in better heat transfer performance, except when the side heaters are too close to the corner where stagnant fluid is deleterious to heat transfer. Fig. 14 shows that the optimal location will change with Ra^*, as well as Ta. Computations are also carried out with fixed side heaters and free shifting of the center heater, as shown in Fig. 15. The optimal

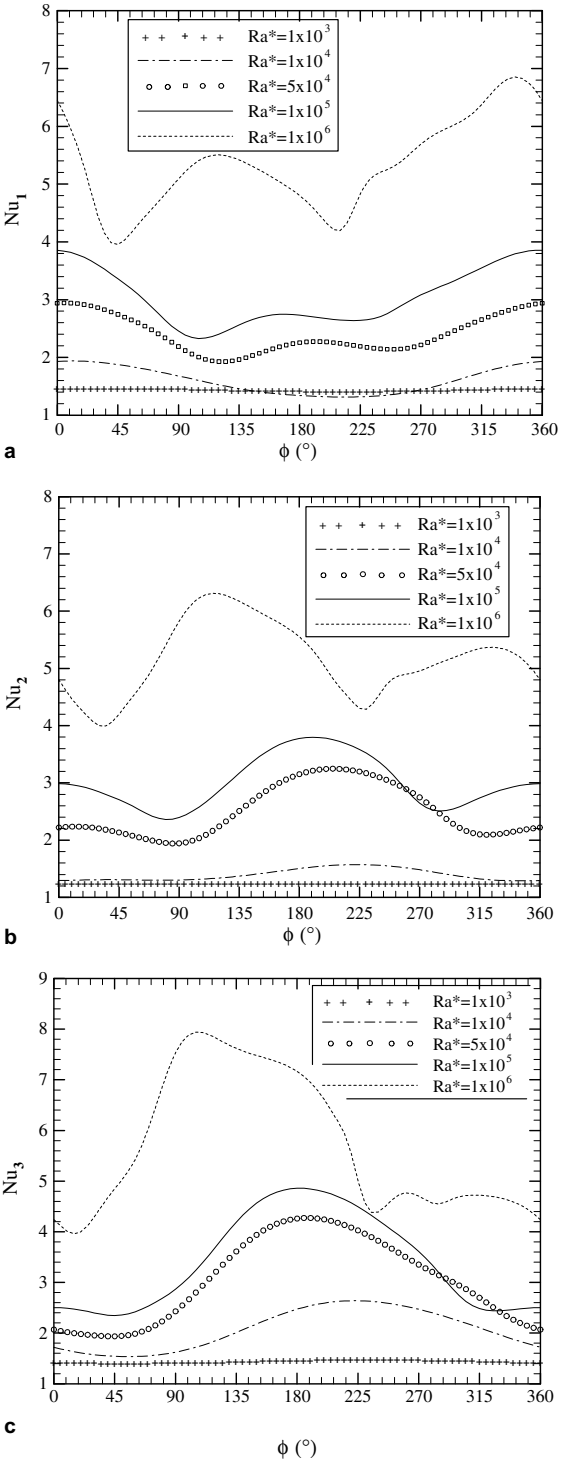

Fig. 11. Mean Nusselt number for each row of heater at different modified Rayleigh numbers ($Ra^* = 1 \times 10^4$, $Pr = 0.7$, $A_W = 1$): (a) row 1, (b) row 2, (c) row 3.

Table 3
Summary of correlations of $\overline{\overline{Nu}}$ at different Ta

$A_W = 1$		
$Ta = 0$	$\overline{\overline{Nu}} = 0.3691Ra^{*0.2028}$	$10^3 \leqslant Ra^* \leqslant 10^7$
$Ta = 10^2$	$\overline{\overline{Nu}} = 0.3367Ra^{*0.2083}$	$10^3 \leqslant Ra^* \leqslant 10^7$
$Ta = 10^3$	$\overline{\overline{Nu}} = 0.2996Ra^{*0.2139}$	$10^3 \leqslant Ra^* \leqslant 10^7$
$Ta = 10^4$	$\overline{\overline{Nu}} = 0.1649Ra^{*0.2505}$	$10^4 \leqslant Ra^* \leqslant 10^7$
$A_W = 2$		
$Ta = 0$	$\overline{\overline{Nu}} = 0.3983Ra^{*0.1930}$	$10^2 \leqslant Ra^* \leqslant 10^6$
$Ta = 10^2$	$\overline{\overline{Nu}} = 0.3184Ra^{*0.2098}$	$10^2 \leqslant Ra^* \leqslant 10^7$
$Ta = 10^3$	$\overline{\overline{Nu}} = 0.2281Ra^{*0.2341}$	$10^3 \leqslant Ra^* \leqslant 10^7$
$Ta = 10^4$	$\overline{\overline{Nu}} = 0.1694Ra^{*0.2506}$	$10^3 \leqslant Ra^* \leqslant 10^7$

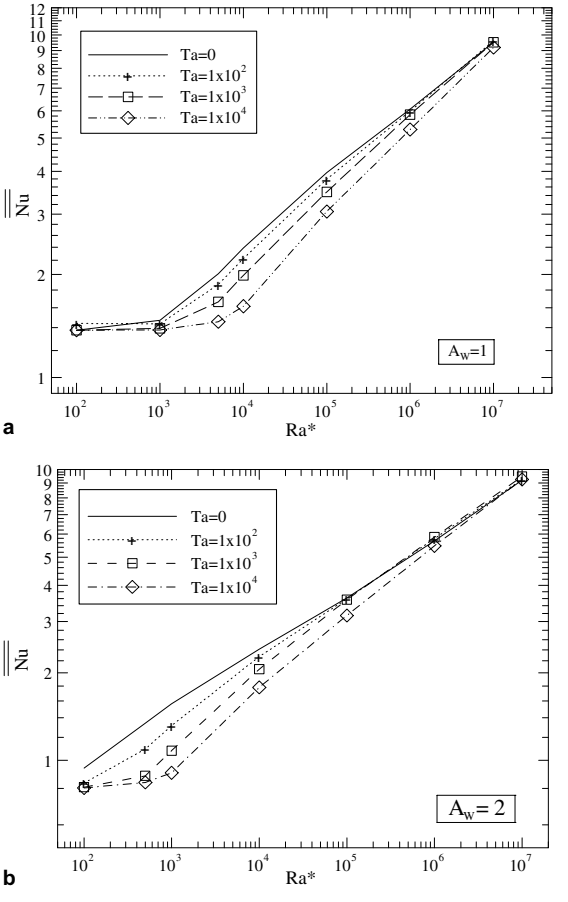

Fig. 12. Effects of Ra^* and Ta on the overall Nusselt number in two aspect ratios.

distribution is not uniform and the heaters are pushed toward the starting cold current of the dominated clock-wise circulation, close to the description by Silva et al. [14] in the stationary situation where the enclosure is dominated by clock-wise circulation. With rotation, the distribution is affected by balancing of clock-wise and counter-clock-wise circulations. The optimal distri-

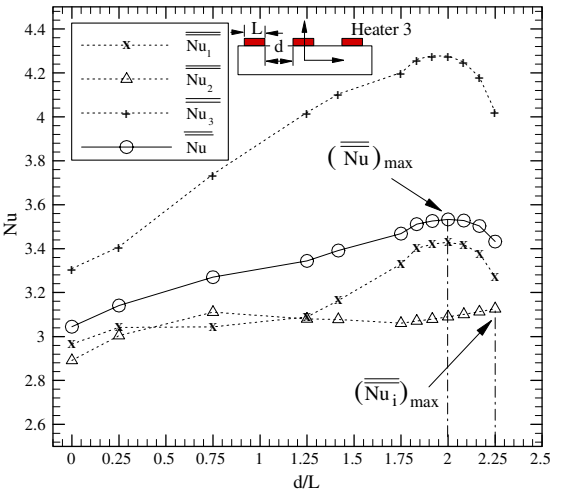

Fig. 13. Results for varying the location of side heaters ($Ra^* = 1 \times 10^5$, $Ta = 1 \times 10^4$, $Pr = 0.7$, $A_W = 1$).

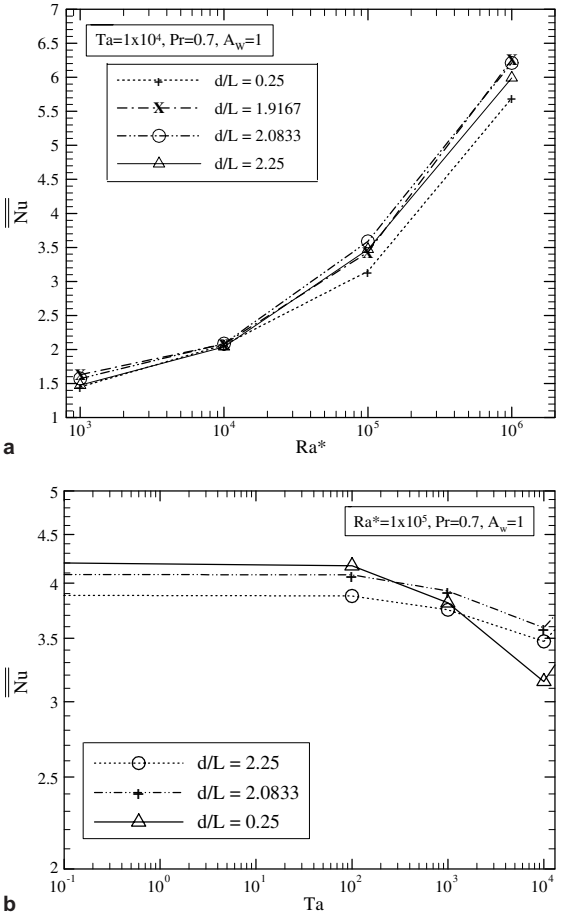

Fig. 14. Effects of Ra^* (a) and Ta (b) to optimal distribution.

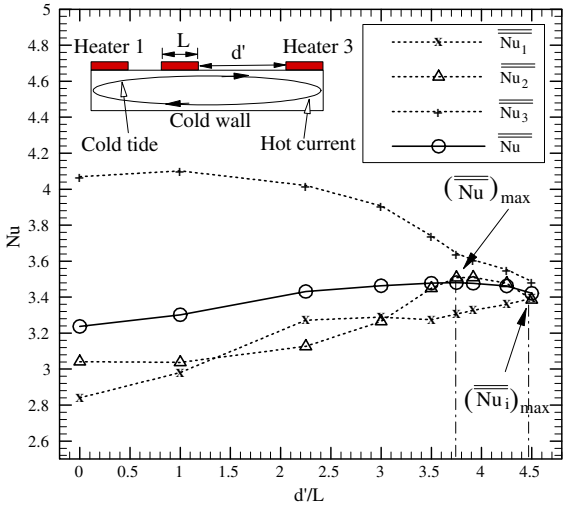

Fig. 15. Results for varying the location of center heaters ($Ra^* = 1 \times 10^5$, $Ta = 1 \times 10^4$, $Pr = 0.7$, $A_W = 1$).

bution of heaters in rotating fluid is close to the results in the stationary situation if they have the same dominant circulation.

4. Conclusions

The following conclusions can be drawn from the present studies:

(1) Three physically realizable phenomena, uni-rotation periodic oscillation, multi-rotation periodic oscillation and chaotic oscillation are identified for rotating discrete heat sources in a cavity.
(2) For the stationary and low rotation cases, thermal buoyancy force causes two or more local peak Nusselt numbers and the flow consists of clock-wise circulation, counter-clockwise circulation and two transition stages between them. With the increase of rotation speed, the clock-wise circulation is enlarged and tends to cover the other circulations. As a result, except for the first local peak *Nu*, the others become weakened and disappeared when the rotation speed is high enough. This process is determined by the relative effects of thermal flux and rotation.
(3) Rotation reduces oscillation in Nusselt number, improves heat transfer in the weak stages but may reduce or increase mean heat transfer performance.
(4) Heat transfer behavior for the two side rows of heaters is in reversed symmetry in the stationary case (shown in Fig. 8(a)), but becomes asymmetrical gradually with the increase of rotation speed.
(5) The correlations between Ra^*, *Ta*, and *Nu* are given in Table 3 for the present conditions.
(6) The optimal distribution of heaters in rotating fluid is close to the results in the stationary situation if they have same dominated clock-wise or counter-clock-wise circulation.

Future work could include effects of aspect ratio, different coolants, experimental investigations considering complex geometrical structure and conjugate heat transfer, or three-dimensional simulations.

References

[1] F.P. Incropera, Convection heat transfer in electronic equipment, J. Heat Transfer 110 (1988) 1097–1111.
[2] M.S. Polentini, S. Ramadhyani, F.P. Incropera, Single phase thermosyphon cooling of an array of discrete heat sources in a rectangular cavity, Int. J. Heat Mass Transfer 36 (1993) 3983–3996.
[3] T.J. Heindel, S. Ramadhyani, F.P. Incropera, Laminar natural convection in a discretely heated cavity: I. Assessment of three-dimensional effects, J. Heat Transfer 117 (1995) 902–909.
[4] T.J. Heindel, F.P. Incropera, S. Ramadhyani, Laminar natural convection in a discretely heated cavity: Comparisons of Experimental and theoretical results, J. Heat Transfer 117 (1995) 910–917.
[5] F.P. Incropera, Liquid Cooling of Electronic Devices by Single-phase Convection, in: Wiley series in thermal management of microelectronic and electronic systems, 1999, pp. 90–124.
[6] S.K.W. Tou, C.P. Tso, X. Zhang, 3-D numerical analysis of natural convective liquid cooling of a 3×3 heater array in rectangular enclosure, Int. J. Heat Mass Transfer 42 (1999) 3231–3244.
[7] R.P. Bobco, Free convection in enclosures exposed to compressive heating, Heat Transfer Therm. Control: Progr. Astronaut. Aeronaut. 78 (1981) 487–515.
[8] L.T. Yeh, Review of heat transfer technologies in electronic equipment, J. Electron. Packag. 117 (1995) 333–339.
[9] Y.L. Lin, T.I.P. Shih, M.A. Stephens, M.K. Chyu, A numerical study of flow and heat transfer in a smooth and ribbed U-Duct with and without rotation, J. Heat Transfer 123 (2001) 219–232.
[10] B.M. Boubnov, G.S. Golitsyn, Convection in Rotating Fluids, Kluwer Academic Publishers, 1995.
[11] S.K.W. Tou, X.F. Zhang, Three-dimensional numerical simulation of natural convection in an inclined liquid-filled enclosure with an array of discrete heaters, Int. J. Heat Mass Transfer 46 (2003) 127–138.
[12] C.P. Tso, L.F. Jin, S.K.W. Tou, X.F. Zhang, Flow pattern evolution in natural convection cooling from an array of discrete heat sources in a rectangular cavity at various orientations, Int. J. Heat Mass Transfer 47 (2004) 4061–4073.
[13] F.J. Hamady, J.R. Lloyd, K.T. Yang, H.Q. Yang, A study of natural convection in a rotating enclosure, J. Heat Transfer 116 (1994) 136–143.

[14] A.K. Silva, S. Lorente, A. Bejan, Optimal distribution of discrete heat sources on a wall with natural convection, Int. J. Heat Mass Transfer 47 (2004) 203–214.
[15] K. Buhler, H. Oertel, Thermal cellular convection in rotating rectangular boxes, J. Fluid Mech. 114 (1982) 261–282.
[16] T.L. Lee, T.F. Lin, Transient three-dimensional convection of air in a differentially heated rotating cubic cavity, Int. J. Heat Mass Transfer 39 (1996) 1243–1255.
[17] J.P. Vanyo, Rotating Fluids in Engineering and Science, Butterworth-Heinemann Press, 1993.
[18] T.L. Yang, L.Q. Wang, Bifurcation and stability of combined free and forced convection in rotating curved ducts of square cross-section, Int. J. Heat Mass Transfer 46 (2003) 613–629.
[19] H.J.S. Fernando, D.C. Smith IV, Vortex structures in geophysical convection, Eur. J. Mech. B/Fluids 20 (2001) 437–470.